17th World Conference on Earthquake Engineering, 17WCEE
Sendai, Japan - September 13th to 18th 2020

SLIP SCALING IN SHALLOW AREAS ABOVE SEISMOGENIC ZONE FOR THE INLAND CRUSTAL EARTHQUAKES

K. Miyakoshi[(1)], N. Inoue[(2)], Y. Matsumoto[(3)], T. Kumamoto[(4)], K. Irikura[(5)], K. Kamae[(6)]

(1) Chief Researcher, Geo-Research Institute, Japan, ken@geor.or.jp
(2) Researcher, Geo-Research Institute, Japan, naoto@geor.or.jp
(3) Researcher, Kozo Keikaku Engineering, Japan, yasuhiro@kke.co.jp
(4) Professor, Okayama University, Japan, tkuma@cc.okayama-u.ac.jp
(5) Adjunct Professor, Aichi Institute of Technology, Japan, irikura@geor.or.jp
(6) Specially-appointed Professor, Institute for Integrated Radiation and Nuclear Science, Kyoto University, Japan, kamae@rri.kyoto-u.ac.jp

Abstract

During the 2016 M_w7.1 Kumamoto earthquake in Japan, strong long-period ground motions with permanent displacements of about 1 - 2 m were observed at Miyazono in Mashiki town and Komori in Nishihara village, respectively. To reproduce these observed long-period ground motions with permanent displacements at near-fault stations, large slips of about 2 - 4 m in shallow areas (LMGAs; Long-period Motion Generation Areas) above the seismogenic zone are needed for simulations of ground motions. Smoothed ramp function with rise time for 2 - 3 s as slip time function is used in LMGAs. For the recipe of strong ground motion prediction, the characterized source model is composed of asperity area and the back ground area in the seismogenic zone. However, this conventional recipe does not always succeed in reproduction of long-period ground motions with permanent displacements which are affected by the large slip in the shallow areas. To update the conventional recipe for the broadband ground motions with permanent displacement in near-fault area, we compiled parameters such as slip and slip velocity time function in LMGAs. We collect 8 source models with LMGAs for 6 inland crustal earthquakes (M_w6.3 - 7.6) and 9 observed permanent displacements at near-source stations for 8 inland crustal earthquakes (M_w6.3 - 7.9). We then find scaling relationships of slip and rise time in LMGA versus seismic moment for the inland crustal earthquakes. Consequently the slip in LMGA is about 2.3 times of the average slip in rupture area and the rise time in LMGA is about 2 times of the empirical scaling relationship of the rise time based on waveform inversion results of strong motion data.

Keywords: source scaling relationships, LMGA (Long-period Motion Generation Area), source time function

1. Introduction

After the 1995 Hyogo-ken Nanbu earthquake (M_w6.9) in Japan, dense strong ground motion networks were installed with about 1000 surface stations (K-NET) at about 20 km intervals and about 700 surface-and-underground stations (KiK-net) by NIED (National Research Institute for Earth Science and Disaster Prevention). Further, seismic-intensity observation networks have been deployed with 600 stations by JMA (Japan Metrological Agency) and with 2900 stations (one for each municipality) by local governments. Since then, strong ground motion data in near-fault area have been accumulated. During the 2016 Kumamoto earthquake (mainshock: M_w7.1, 16th. April), strong long-period ground motions with permanent displacements of about 1 - 2 m were observed at Miyazono in Mashiki town (93051) and Komori in Nishihara village (93048), respectively. To reproduce these long-period ground motions with permanent displacements of the seismograms recorded at near-fault stations, Irikura *et al*. (2019) [1] showed that the LMGAs (Long-period Motion Generation Areas) in shallow areas above seismogenic zones with large slip of about 2 - 4 m are needed. They assumed the smoothed ramp function with rise time for 2 - 3 s as slip velocity time function in LMGAs.

Irikura and Miyake (2011) [2] proposed the recipe for strong ground motion prediction using the characterized source model composed of several areas having large slip (asperity area) and the back ground area with less slip in the seismogenic zones. The asperities have high stress drop and generate strong ground motions, being called strong-motion generation areas (SMGAs) (Miyake et al., 2003 [3]). Iwaki *et al*. (2016) [4] validated this conventional recipe using hybrid simulations of crustal earthquakes (M_w6.6: 2000 Tottori; 2004 Chuetsu) in Japan. The examined results are satisfactory showing a good agreement between simulated waveforms and observed ones. This conventional recipe is based on the 3 stage scaling relationship by HERP (2017) [5]. For the first stage, the rupture area (A) is proportional to $Mo^{2/3}$ (self-similar scaling) for earthquakes smaller than M_w6.5 (Somerville *et al*. 1999 [6]). For the second stage where fault width saturate for the limited thickness of the seismogenic zones, A is proportional to $Mo^{1/2}$ for earthquakes between around M_w6.5 and 7.4 (Irikura and Miyake 2011 [2]). Hashimoto (2007) [7] showed that rupture widths for inland crustal earthquakes ($M_w \geq$ around 6.5) saturate at about 16 - 18 km for the thickness of the seismogenic zones using selected reliable data compiled by Stirling *et al*. (2002) [8]. Murotani *et al*. (2015)[9] proposed the third stage scaling relationship of source parameters for large crustal earthquakes in "megafault" systems, including earthquakes with magnitudes larger than M_w7.4. For the third stage, A is proportional to Mo (the saturation of the slip) for earthquakes larger than M_w7.4. Tajima *et al*. (2013) [10] showed a saturation of the average slip of about 3 m in the rupture area of earthquakes ($M_w \geq$ 7.4) retrieved from heterogeneous slip distribution source models estimated by waveform inversion results of strong motion data.

However, the conventional recipe does not always succeed in simulating long-period ground motions with permanent displacement which are affected by the large slip in the shallow areas for large earthquakes with surface rupturing. To update the conventional recipe for the broadband ground motions with permanent displacement in near-fault area, we comipled the parameters such as slip and rise time in LMGAs. We collected 8 source models with LMGAs for 6 inland crustal earthquakes (M_w6.3 - 7.6) and 9 observed permanent displacements at near-fault stations for 8 inland crustal earthquakes (M_w6.3 - 7.9). We then proposed the scaling relationships of parameters such as slip and rise time in LMGA versus seismic moment for the inland crustal earthquakes with reference to the 3 stage scaling relationship by HERP (2017) [5].

2. Scaling relationship of slip in LMGA

2.1 Permanent displacement at hanging wall side and footwall side

Permanent displacement (D_P) recorded at near-fault stations is one side slip at the hanging wall (HW) side or the footwall (FW) side. For strike-slip fault, the permanent displacment of the horizontal component is ideally equal to the slip at HW side (D_{HW}) and the one at FW side (D_{FW}), respectively (i.e., $D_P = D_{HW} = D_{FW}$) (see Fig.1). Both side slip ($|D_{HW}|+|D_{FW}|$) denotes the fault slip in shallow areas taken as the direction of the hanging wall side (HW), relative to the footwall side (FW). In generale fault displacment (D_{fd}) is also equal to both side of the permanent displacement ($|D_{P(HW)}|+|D_{P(FW)}|$) (see Fig.1). Kamai *et al*. (2014) [11] showed

the distribution of the normalized fling-step amplitude (D_{site}/D_{fault}), in which D_{site} is the fling step amplitude and D_{fault} is the average slip in rupture area. Fling-step amplitude (D_{site}) is equal to the permanent displacement (D_P) at extremely near-fault area. In this study we focus to reproduce the large permanent displacements at extremely near-fault area, which are affected from fault slips in shallow areas, little affected from fault slips in deeper part of rupture areas. For this reason we used slip in shallow areas ($|D_{HW}|+|D_{FW}|$) for normalization in this study, although Kamai *et al*. (2014) used the average slip in rupture area (D_{fault}) for normalization. Therefore, the normalized fling-step amplitude (D_{site}/D_{fault}) is converted into the ratio of ($D_P/(|D_{HW}|+|D_{FW}|)$). In the same idea as Kamai *et al*. (2014) [11] using the hybrid simulation method (Graves and Pitarka, 2010 [12]), the ratio by the equation of (1) is about 0.5 extremely near surface-fault ruptures for the strike-slip fault:

$$D_P / (|D_{HW}| + |D_{FW}|) = 0.5 \text{ for the horizontal component of the strike-slip fault} \quad (1)$$

The ratio by the equation of (2) for the vertical component at HW side is about 0.7 extremely near surface-fault ruptures for the reverse fault in the same idea as Kamai *et al*. (2014) [11]:

$$D_P / (|D_{HW}| + |D_{FW}|) = 0.7 \text{ for the vertical component of the reverse fault} \quad (2)$$

On the other hand, Kamai *et al*. (2014) [11] showed that the normalized fling-step amplitude (D_{site}/D_{fault}) at FW side is less than about 0.1 for the reverse fault. It is noted that the very small ratio (< 0.1) at FW side possibly increases measuring errors and then we adopt only equation (2) at HW side for the reverse fault. We use above two equations in Section 2.3 for estimation of slip in LMGA using the observed permanent displacements for strike-slip fault and reverse fault.

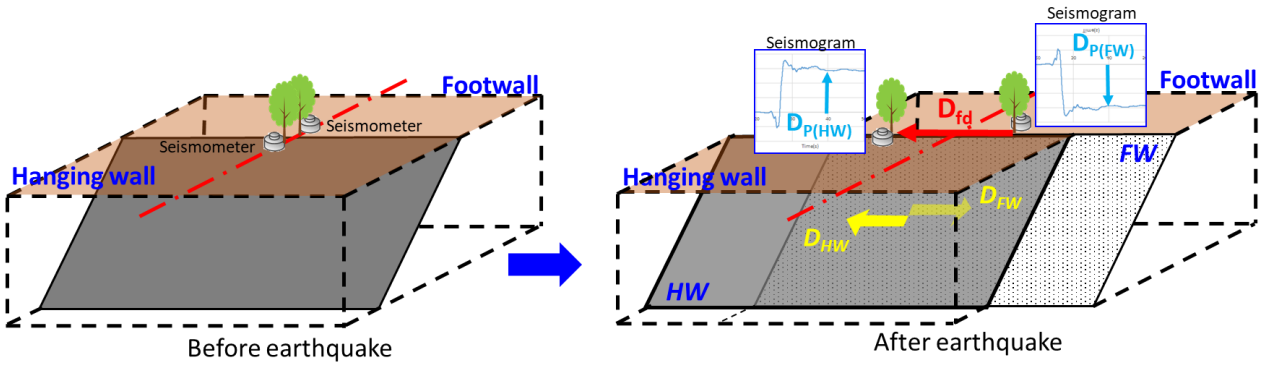

Fig.1 Schematic figure of slip at hanging wall (D_{HW}) and the one at footwall side (D_{FW}). D_P denotes the permanent displacement of seismograms at near-fault station. D_{fd} denotes the fault displacement.

2.2 Source models and slip in LMGA

Eight source models with LMGAs for 6 earthquakes (M_w6.3 - 7.6) are compiled for investigation of slip in LMGAs (see Table 1 [1], [13] - [19]). Fig.2 shows the distribution map of target earthquakes in this study. All of the six crustal earthquakes have surface fault ruptures. Matsumoto *et al*. (2018) [15] estimated slip time functions in LMGAs using the smoothed ramp function with a trial and error method to reproduce the long-period ground motions with permanent displacements at near-fault stations. Tanaka *et al*. (2018) [16] also modeled slip velocity time functions in LMGAs using the trianguler or the Yoffe-type functions (Tinti *et al*., 2005 [20]) based on the waveform inversion results of strong motion data. Average slip in rupture area (D_{sub_ave}) is also shown in Table 1. Fig.3 shows the comparison between slip in LMGA (D_{LMGA}) and average slip in rupture area (D_{sub_ave}). We recognized that the ratio of the slip in LMGA to the average slip in rupture area (D_{LMGA}/D_{sub_ave}) is about 2.3 (see Table 1).

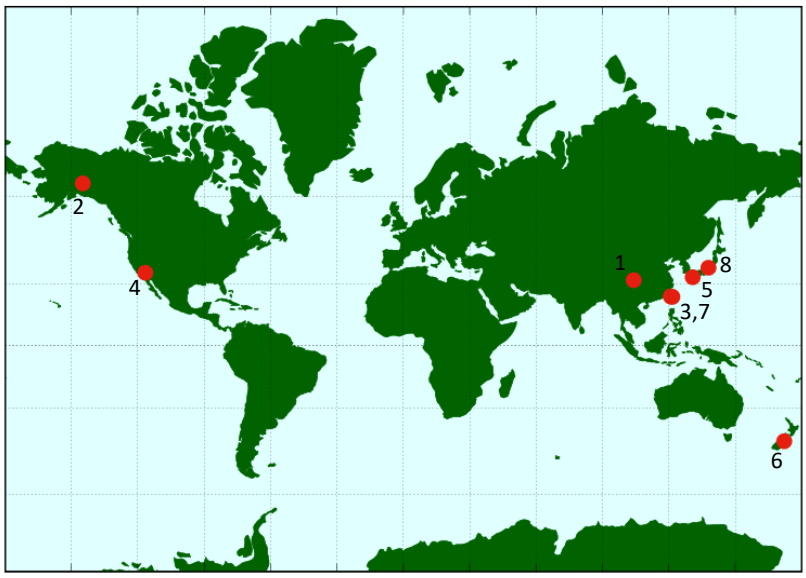

Fig.2 Distribution map of target earthquakes in this study. Numbers in this figure correspond earthquakes in Table 1

Table 1 Slip parameters in LMGAs based on the foward modeling and waveform inversion results

No.	EQ. name	Mo[Nm]	CMT catalog	Mw	Type	Av. slip in rupture area (D_{sub_ave})	LMGA					
							D_{LMGA} [m]	D_{LMGA}/D_{sub_ave}	Av. rise time [s]	Slip velocity or time function	Target sites	References
1	2008 Wenchuan	8.97E+20	GCMT	7.9	RV	3.2	-	-	-	-	-	-
2	2002 Denali	7.48E+20	GCMT	7.8	SS	4.3	-	-	-	-	-	-
3	1999 Chi-Chi	3.38E+20	GCMT	7.6	RV	4.3	10.2#	2.4	6.0#	Triangle*	TCU052, TCU068	Kaneda et al. (2017) [13]
4	1992 Landers	1.06E+20	GCMT	7.3	SS	2.7	4.7	1.7	3.6	Triangle*	LUC	Tanaka et al. (2017) [14]
5	2016 Kumamoto (Main shock)	4.42E+19	F-net	7.1	SS	1.7	4.0	2.4	2.5	Smoothed ramp	KMMH16, Nishihara (93048), Mashiki (93051), etc	Matsumoto et al. (2018) [15]
							4.1	2.5	3.0	Regularized Yoffe (Model-02)	KMMH16, Nishihara (93048), etc	Tanaka et al. (2018) [16]
6	2010 Darfield	3.64E+19	GCMT	7.0	SS	0.8	2.6	3.3	4.0	Smoothed ramp (Model D3)	GDLC, ROLC, etc	Irikura et al. (2019) [1]
7	2018 Hualien	4.53E+18	GCMT	6.4	OB	0.5	1.0	2.0	1.5	Smoothed ramp (Fault 2)	HWA019 etc.	Miyakoshi et al. (2019) [17]
8	2014 Nagano Hokubu	2.76E+18	F-net	6.3	RV	0.5	1.0	2.2	3.0	Smoothed ramp	NGNH36 etc.	Matsumoto et al. (2019) [18]
							0.8	1.8	2.5	Triangle*	NGNH36	Tanaka et al. (2017) [19]

RV: Reverse, SS: Strike, OB: Oblique #: average Triangle*: Tanaka personal com.

Average (D_{LMGA}/D_{sub_ave}) = 2.3

2.3 Slip in LMGA estimated from observed permanent displacement

For the purpose of expanding data of the slips in LMGA, we investigated 9 observed permanent displacements at the seismometers within about 2 km from the surface-fault ruptures for 8 earthquakes (M_w6.3 - 7.9) in this study (Table 2 [1], [15], [17], [18], [21], [22]). Permanent displacement (D_P) in Table 2 shows slips in vertical component for reverse fault and ones calculated by vector sum of two horizontal components for strike-slip fault. We calculated permanent displacement by vector sum of two horizontal components and vertical component for oblique-slip fault.

Slip of LMGA (D_{LMGA}) is both side slip ($|D_{HW}|+|D_{FW}|$) taken as the direction of the hanging wall side (HW), relative to the footwall side (FW) in shallow areas above the seismogenic zones. Therefore, equations (1) and (2) are converted into (3) and (4), respectively.

$D_P / D_{LMGA} = 0.5$ for the horizontal component of the strike-slip fault (3)

$D_P / D_{LMGA} = 0.7$ for the vertical component of the reverse fault (4)

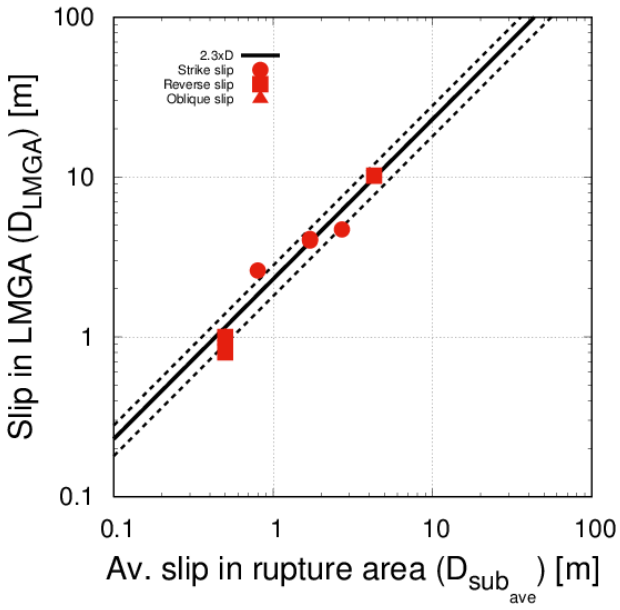

Fig.3 Comprison between slip in LMGA and average slip in rupture area (D_{LMGA} - D_{sub_ave}) (see Table 1). Black solid line shows $2.3 \times D_{sub\_ave}$. Two broken lines show 2 times and 0.5 times of black solid line.

Table 2 Observed permanent displacement of seismograms at near-fault stations (< about 2km)

No.	EQ. name	Mo[Nm]	Type	D_{LMGA} [m] (Table 1)	Observed permanent displacements of seismograms (D_P) at near-fault stations				
					D_P [m]	Station	Surafce-fault distance [km]	Condition	References
1	2008 Wenchuan	8.97E+20	RV	-	0.8	MZQ#	1.7	HW	Lu et al. (2010) [21]
					3.8	SFB#	1.2	HW	
2	2002 Denali	7.48E+20	SS	-	3.1	MEN(GPS)*	unknown	-	Asano et al. (2005) [22]
3	1999 Chi-Chi	3.38E+20	RV	10.2	4.5	TCU068#	0.3	HW	Lu et al. (2010) [21]
4	1992 Landers	1.06E+20	SS	4.7	4.3	Lucerne**	2.2	-	Lu et al. (2010) [21]
5	2016 Kumamoto (Main shock)	4.42E+19	SS	4.0 4.1	1.5	Nishihara** (93048)	1	-	Matsumoto et al. (2018) [15]
6	2010 Darfield	3.64E+19	SS	2.6	1.5	GDLC**	1	-	Irikura et al. (2019) [1]
7	2018 Hualien	4.53E+18	OB	1.0	0.5	HWA019***	0.5	HW	Miyakoshi et al. (2019) [17]
8	2014 Nagano Hokubu	2.76E+18	RV	1.0 0.8	0.05	NGNH36#	2	FW	Matsumoto et al. (2019) [18]

RV: Reverse, SS: Strike, OB: Oblique

*: one horizontal component **: vector sum (two horizontal components)
***: vector sum (two horizontal and vertical components)
#: vertical component

Fig.4 shows the comparison between slip in LMGA (D_{LMGA}) and permanent displacement (D_P) of the seismograms within about 2 km from surface-fault ruptures for the same event. Red solid line in Fig.4(a) shows $0.5 \times D_{LMGA}$ for strike-slip fault and black one in Fig.4(b) shows $0.7 \times D_{LMGA}$ for reverse fault. Data of vertical component of permanent displacement (D_P) at NGNH36 (KiK-net station) are omitted (crosses in Fig.4(b)) in this study because of low accuracy at FW site. We recognized that relationship between the slip

in LMGA (D_{LMGA}) and the observed permanent displacement (D_P) have almost good agreement with about 0.5 for strike-slip fault or about 0.7 at HW side for reverse fault. It is suggested that slip in LMGA is estimated from the observed permanent displacement at near-fault stations (i.e., $D_{LMGA} \cong 2 \times D_P$ for strike-slip fault; $D_{LMGA} \cong 1.4 \times D_P$ for revserse fault and oblique-slip fault). Thus we used the slip in LMGA (D_{LMGA}) estimated from the observed permanent displacements (D_P) at near-fault stations for investigation of relationship of slip in LMGA versus seismic moment.

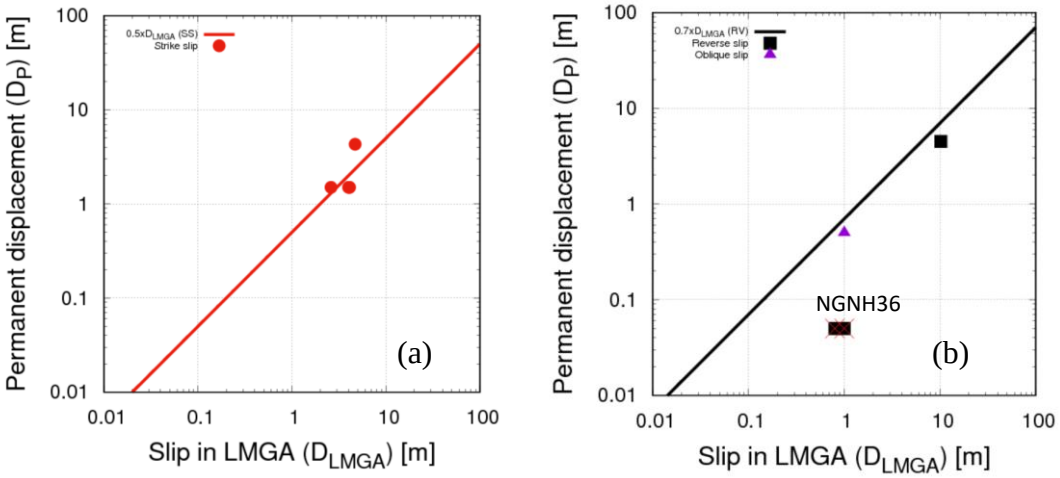

Fig.4 Comprison between permanent displacement of seismomograms and slip in LMGA (D_P -D_{LMGA}). (a) Strike-slip fault type (red solid line: $0.5 \times D_{LMGA}$), (b) Reverse fault and obliqe-slip fault type (black solid line: $0.7 \times D_{LMGA}$)

2.4 Empirical scaling relationship of the maximum fault displacement versus seismic moment

Matsuda (1975) [23] proposed the empirical relationships between the maximum fault displacements (D_{fd}) and JMA magnitude (M_J). He used past 14 inland crustal earthquakes (1891 - 1970) in Japan. Applying the empirical relationship between JMA magnitude (M_J) and seismic moment (Mo) (Takemura, 1990 [24]), the empirical relationship of D_{fd} versus M_J is converted into that of D_{fd} versus Mo.

$$\log_{10} D_{fd}\,[\mathrm{m}] = 0.5123 \times \log_{10} \mathrm{Mo}\,[\mathrm{Nm}] - 9.4974 \qquad (5)$$

It is noted that the slope of this scaling relationship (D_{fd} - Mo) is roughly 0.5. We then validated this empirical relationship using inland crustal earthquakes ($M_w > 6$) which occurred from 1857 to 2008 including recent earthquakes (Wesnousky, 2008 [25]; Murotani *et al.*, 2015 [9]). Fig.5 shows the scaling relationship between the maximum fault displacement (D_{fd}) and seismic moment (Mo). We also compiled the maximum fault displacements of the 2014 Nagano-Hokubu earthquake (M_w6.3: Ishimura *et al.*, 2015 [26]) and the 2016 Kumamoto earthquake (M_w7.1: Shirahama *et al.*, 2016 [27]) in Fig.5. Observed maximum fault displacements have a good agreement with the empirical scaling relationship of maximum fault displacement versus seismic moment, although they vary widely.

2.5 Empirical scaling relationship of slip in LMGA versus seismic moment

We compared the empirical scaling relationship of the maximum fault displacement versus slip in LMGAs (see Fig.6). Solid symbols show slips in LMGAs and open ones show slips in LMGAs estimated from the relationships in this study ($D_{LMGA} \cong 2 \times D_P$ for strike-slip fault; $D_{LMGA} \cong 1.4 \times D_P$ for revserse fault and oblique-slip fault) in Fig.6. We omitted the slip for the vertical component in LMGA estimated from the very small permanent displacement (0.05 m) observed at NGNH36 (FW side) because of the possibility of low accuracy (cross in Fig.6). It seems that estimated slips in LMGAs (open symbols in Fig.6) are saturated over M_w7.5

except for MZQ station of the 2008 Wenchuan earthquake. Because MZQ is located between two segments (Beichuan and Wenchuan segments, Lu *et al*., 2010 [21]), permanent displacement at MZQ possibly reduced at the end of segment (e.g., Wesnousky, 2008 [25]). Slips in LMGAs (6 ~ M_w ~ 7.5) have a good agreement with the empirical scaling relationship of the maximum fault displacement versus seismic moment (black thick solid line in Fig.6). Red solid line in Fig.6 shows the relationship between average slip in rupture area (D_{sub_ave}) and seismic moment (Mo). This scaling relationship (D_{sub_ave} - Mo) is obtained from another scaling relationship between rupture area and seismic moment (*A* - Mo) for the 2nd stage (HERP, 2017 [5]) assuming J-SHIS velocity structure model (2019 [28]: Layer 33, Vs=3400m/s, ρ=2750kg/m^3, μ=31.8GPa).

$$\log_{10} D_{sub\_ave}\,[\mathrm{m}] = 0.5\times\log_{10} \mathrm{Mo}[\mathrm{Nm}] - 9.6297 \quad \text{(red solid line in Fig.6)} \qquad (6)$$

The slope of this scaling relationship (D_{sub_ave} - Mo) for the 2nd stage is 0.5. It is noted that slope of the scaling relationship of D_{fd} - Mo is almost equal to that of D_{sub_ave} - Mo. Red broken line in Fig.6 shows 2 times of the scaling relationship (D_{sub_ave} - Mo) for the 2nd stage. We recognized that 2 times of the scaling relationship (D_{sub_ave} - Mo) for the 2nd stage (red broken line in Fig.6) is almost equal to the empirical scaling relationship of the maximum fault displacement (D_{fd}) versus seismic moment (black solid line in Fig.6). Finally slip in LMGA (D_{LMGA}) is almost equal to about 2.3 time of the average slip in rupture area (D_{sub_ave}). Because average slip in asperity area (D_{asp}) is set to 2 times of the average slip in rupture area (D_{sub_ave}) (HERP, 2017 [5]), slip in LMGA is almost equal to the average slip in asperity area.

$$D_{LMGA} = 2.3\times D_{sub\_ave} \ (\cong D_{asp}) \qquad (7)$$

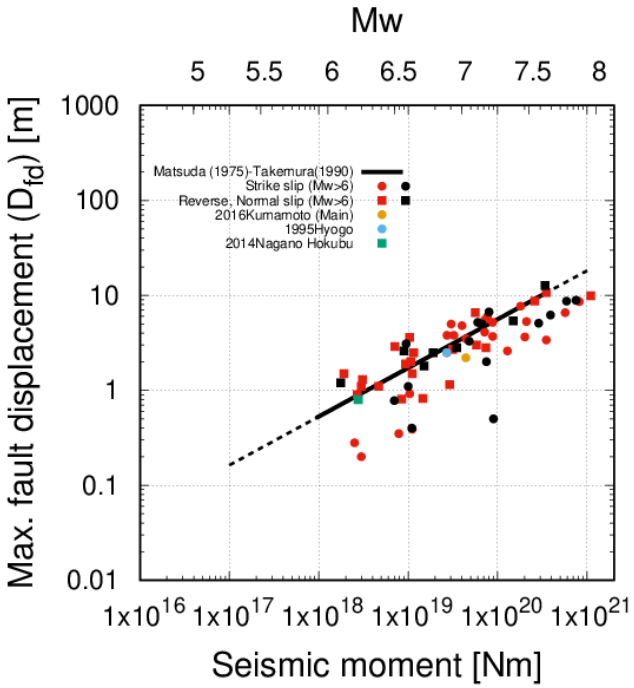

Fig.5 Scaling relationship of the maximium fault displacement versus seismic moment (D_{fd} - Mo) (Matsuda, 1975[23]: Takemura, 1990 [24]). Red symbols denote data collected by Murotani *et al*. (2015) [9] and black ones collected by Wesnousky (2008) [25].

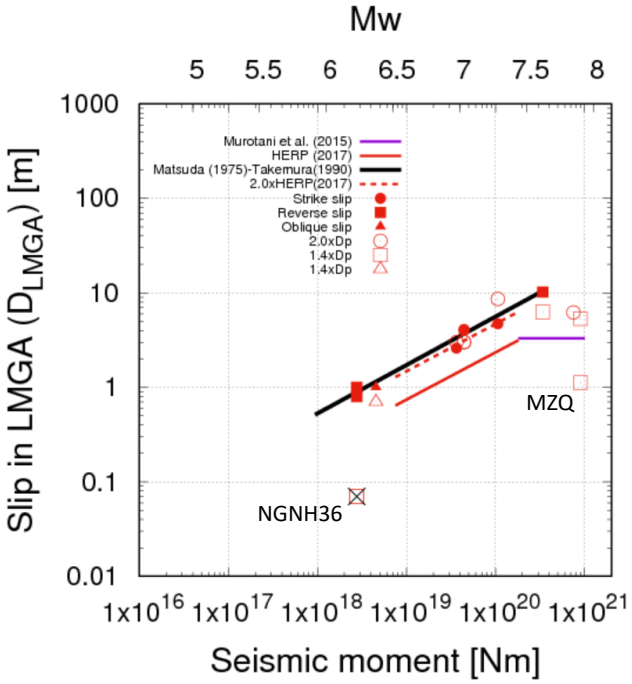

Fig.6 Scaling relationship of slip in LMGA versus seismic moment (D_{LMGA} - Mo). Red symbols denote slip in LMGAs estimated from source models, open ones denote slip estimated from the permanent displacements.

3. Empirical scaling relationship of rise time in LMGA versus seismic moment

Eight source models with LMGAs for 6 earthquakes (M_w6.3 - 7.6) are used for investigation of rise time (Tr_{LMGA}) in LMGAs (see Table 1). To investigate the scaling relationship of rise time in LMGA versus seismic moment, we compared these data and existing empirical scaling relationships [6, 11, 29-31]. Fig.7 shows comparison between rise time data and exiting empirical scaling relationships. Somerville *et al.* (1999) [6] proposed scaling relationship of rise time based on the waveform inversion results of strong motion data (black solid line in Fig.7). Two times of the scaling relationship of rise time (Somerville *et al.*, 1999[6]) is also plotted as red sloid line in Fig.7. Except for Somerville *et al.* (1999)[6], other empirical scaling relationships [11, 29-31] are estimated using forward modeling for representation by a ramp time function fitting observed displacement or velocity seismograms at near-fault stations. Excluding 2014 Nagano-Hokubu earthquake (M_w6.3; squares in Fig.7), rise times in LMGAs have a good agreement with 2 times of the empirical scaling relationship of rise time (Somerville *et al.*, 1999[6]). Because vertical component permanent displacement (D_P) at NGNH36 (KiK-net station) is very small as previously mentioned, estimated slip time function has possibly low accuracy. Except for the 2014 Nagano-Hokubu earthquake, we recognized that rise times in LMGAs almost agree about 2 times of the empirical scaling relationship of rise time by Somerville *et al.* (1999) [6].

Recipe for strong motion prediction (HERP,2017[5]) adopted Nakamura and Miyatake (2000) [32] as slip velocity time function: the Kostrov-like slip velocity time functions are assumed to be functions of the peak slip velocity and rise time (Tr) based on the dynamic simulation results of Day (1982) [33]. Rise time in asperity area (Tr_{asp}) is evaluated by HERP (2017 [5]):

$Tr_{asp} = \alpha \times W_{asp}/V_r$ (α: 0.5, V_r: rupture propagation velocity, W_{asp}: width of asiperity area)

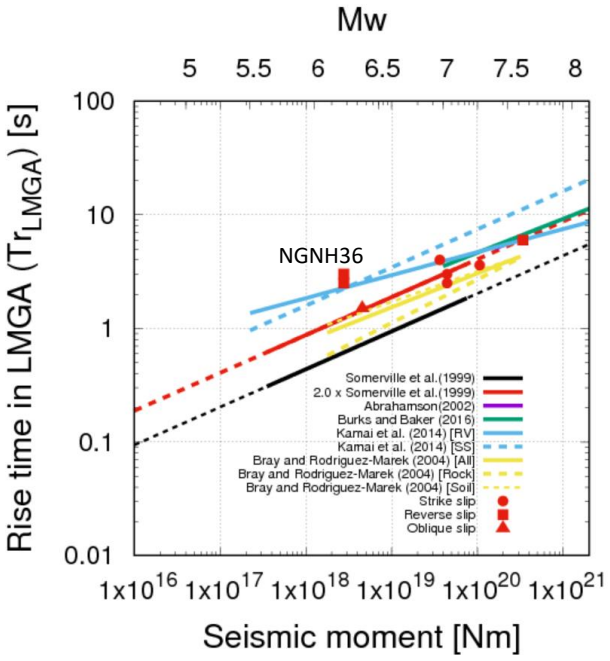

Fig.7 Scaling relationship of rise time in LMGA versus seismic moment (Tr_{LMGA} - Mo). Red symbols denote slip in LMGAs estimated from source models.

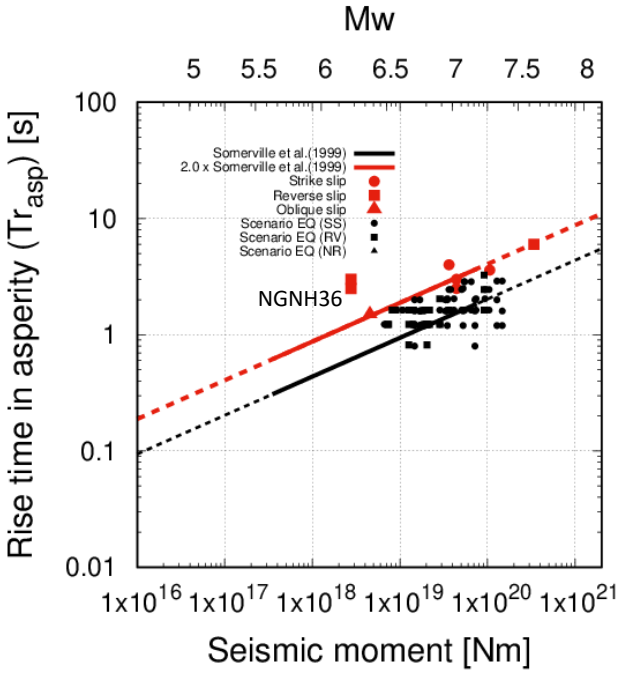

Fig.8 Comparison between rise time in asperity area (Tr_{asp}) of the characterized source models of scenario earthquakes (black symbols) and that predicted by the scaling relationship (black line) by Somerville *et al*., (1999) [6]. Rise times in LMGAs (Tr_{LMGA}) are also plotted as red symbols.

We compiled rise time in asperity area (Tr_{asp}) using the source parameters of the characterized source models of scenario earthquakes (M_w6.5 - 7.4: 2nd stage) estimated by HERP (2017[34], 2018[35]). Fig.8 shows a comparison between rise time in asperity area (Tr_{asp}) of the characterized source models of scenario

earthquakes and that predicted by the scaling relationships (Somerville *et al*.,1999 [6]). Rise times in LMGAs (Tr_{LMGA}) are also plotted in Fig.8. Rise times in asperity area (Tr_{asp}) of the characterized source models of scenario earthquakes are almost agreement with the empirical scaling relationship of rise time (black solid line in Fig.8) by Somerville *et al*. (1999) [6], although they have large scatters. Consequently we recognized that rise time in LMGA is almost equal to 2 times of that in asperity area of characterized source model by HERP(2017 [5]).

$$Tr_{LMGA} \cong 2 \times Tr_{asp} \quad (9)$$

4. Conclusions

During the 2016 Kumamoto earthquake (mainshock; M_w7.1), strong long-period ground motions with permanent displacements of about 1 - 2 m were observed at Miyazono in Mashiki town (93051) and Komori in Nishihara village (93048), respectively. To reproduce these observed long-period ground motions with permanent displacements at near-fault stations, large slips of about 2 - 4 m in shallow areas (LMGAs; Long-period Motion Generation Areas) above the seismogenic zones are needed. Smoothed ramp function with rise time for 2 - 3 s as slip time function is used in LMGAs. For the recipe of strong ground motion prediction, the characterized source model is composed of several areas having large slip (asperity area) and the background area with less slip. However, this conventional recipe does not always succeed in simulating long-period ground motions with permanent displacement which are affected by the large slip in the shallow areas. To update the conventional recipe for the broadband ground motions with permanent displacement in near-fault area, we compiled the parameters such as slip and slip velocity time function in LMGAs. We collected 8 source models with LMGAs for 6 inland crustal earthquakes (M_w6.3 - 7.6) and 9 observed permanent displacements at near-fault stations for 8 inland crustal earthquakes (M_w6.3 - 7.9). We propose the scaling relationships of parameters in LMGA for the inland crustal earthquakes. Slip in LMGA is recognized to be about 2.3 times of average slip in rupture area. We poposed 2.3 times of the average slip in rupture area for the 2nd stage of the empirical scaling relationship (HERP, 2017[5]). Slip in LMGA is almost equal to the average slip in asperity area of the characterized source model (HERP, 2017[5]). We also proposed that rise time in LMGA is about 2 times of rise time for the empirical scaling relationship based on wavform inversion results of strong motion data (Somerville *et al*., 1999[6]). Rise time in LMGA is recognized to be almost equal to 2 times of that in asperity area of the characterized source model (HERP, 2017[5]).

However, the number of large earthquakes with surface rupture used in this study is not suffcient for discussing uncertainties. We need to compile more informations of slip velocity time function of LMGAs for updating of the proposed scaling relationship of LMGA in this study, and to reproduce very-near-fault motions for validating simulation of broadband ground motions with permanent displacement.

5. Acknowledgements

We would like to thank Dr. Tanaka, S (TEPSCO) for provision of slip velocity time functions in LMGAs. This study was based on the 2019 research project “Examination for uncertainty of strong ground motion prediction for inland crustal earthquakes” by The Secretariat of the Nuclear Regulation Authority (NRA), Japan.

6. References

[1] Irikura K, Kurahashi S, Matsumoto Y (2019): Extension of characterized source model for long-period ground motions in near-fault area, *Pure Appl. Geophys.*, https://doi.org/10.1007/s00024-019-02283-4.

[2] Irikura K, Miyake H (2011): Recipe for predicting strong ground motion from crustal earthquake scenarios. *Pure Appl. Geophys.*, ***168***, 85-104.

[3] Miyake, H, Iwata T, Irikura K (2003): Source characterization for broadband ground-motion simulation: kinematic heterogeneous source model and strong motion generation area, *Bull. Seismol. Soc. Am.*, ***93***, 6, 2531-2545.

[4] Iwaki A, Maeda T, Morikawa N, Miyake, H, Fujiwara H (2016): Validation of the recipe for broadband ground-motion simulations of Japanese crustal earthquakes, *Bull. Seismol. Soc. Am.*, ***106***, 5, 2214-2232.

[5] Headquarters for Earthquake Research Promotion (HERP) (2017): Predicting strong ground motions for identified earthquake scenarios (RECIPE) (in Japanese). https://www.jishin.go.jp/main/chousa/17_yosokuchizu/recipe.pdf.

[6] Somerville P, Irikura K, Graves G, Sawada S, Wald D, Abrahamson N, Iwasaki Y, Kagawa T, Smith N, Kowada A (1999): Characterizing crustal earthquake slip models for the prediction of strong ground motion, *Seismological Research Letter*, ***70***, 59–80.

[7] Hashimoto T (2007): The surface length of earthquake fault and the moment magnitude, In *Abstracts of Japan Geoscience Union meeting*, S145-013.

[8] Stirling M, Rhoades D, Berryman K (2002): Comparison of earthquake scaling relations derived from data of instrumental and pre preinstrumental era, *Bull. Seismol. Soc. Am.*, ***92***, 2, 812-830.

[9] Murotani S, Matsushima S, Azuma T, Irikura K, Kitagawa S (2015): Scaling relation of source parameters of earthquakes on inland crustal mega-fault systems, *Pure Appl. Geophys.*, 172, 1371-1381.

[10] Tajima R., Matsumoto Y, Si H, Irikura K (2013): Comparative study on scaling relations of source parameters for great earthquakes in inland crusts and on subducting plate-boundaries, *ZISIN2* (*Journal of Seismological Society Japan*), ***66***, 31-45 (in Japanese with English abstract).

[11] Kamai R, Abrahamson N, and Graves R (2014): Adding fling effects to processed ground-motion time histories, *Bull. Seismol. Soc. Am*. ***104***, 4, 1914-1929.

[12] Graves RW, Pitarka A (2010): Broadband ground-motion simulation using a hybrid approach, *Bull. Seismol. Soc. Am*. ***100***, 5A, 2095-2123.

[13] Kaneda J, Tanaka S, Hikima, K, Hisada Y (2017): Estimation of slip velocity function for the region shallower than seismogenic layer, Part1, Study on slip velocity functions of the 1999 Chi-Chi earthquake, In *Summaries of technical papers of annual meeting, AIJ*, 21146.

[14] Tanaka S, Kaneda J, Hikima, K, Hisada Y (2017): Estimation of slip velocity function for the region shallower than seismogenic layer, Part2, An approximate expression of slip velocity function based on the regularized Yoffe function, In *Summaries of technical papers of annual meeting, AIJ*, 21147.

[15] Matsumoto H, Miyakoshi K, Takahama T (2018): Characterized source model for evaluating long-period (more than 2s-) ground motion including permanent displacement of the 2016 Kumamoto earthquake (Mj7.3). *The 15th Japan Earthquake Engineering Symposium*, PS1-01-17.

[16] Tanaka S, Kaneda J, Hikima K, Hisada Y (2018): Characterized fault model for prediction of long-period ground motions containing permanent displacement in the near-fault region, *J. Struct. Constr. Eng., AIJ*, ***83***, 752, 1525-1535.

[17] Miyakoshi K, Matsumoto Y, Yamada S, Mori J, Cho I, Hayashida T, Kuo CH, Ling CM, Yen YT, Kuo KC, Guo Y (2019): Estimation of underground structures around source area of the 2018 Hualien, Taiwan, earthquake (Mw6.4) using microtremor array observations, In *Abstract of the 2019 Seismological Society of Japan fall meeting*, S16P-05.

[18] Matsumoto Y, Miyakoshi K, Irikura K (2019): Characterized source model for evaluating long-period (more than 2s-) ground motion during the 2014 Northern Nagano earthquake (Mj 6.7), In *Abstract of the 2019 Seismological Society of Japan fall meeting*, S15P-09.

[19] Tanaka S, Hikima K, Hisada Y (2017): Slip velocity time function for shallower region than the seismogenic layer based on source fault models, *Journal of Japan Association for Earthquake Engineering*, ***15***, 5, 141–156 (in Japanese with English abstract).

[20] Tinti E, Fukuyama E, Piatanesi A, Cocco M (2005): A kinematic source-time function compatible with earthquake dynamics, *Bull. Seismol. Soc. Am.*, ***95***, 4, 1211-1223.

[21] Lu M., Li XJ, An XW, Zhao JX (2010): A preliminary study on the near-source strong-motion characteristics of the great 2008 Wenchuan earthquake in China, *Bull. Seismol. Soc. Am*. ***100***, 5B, 2491–2507.

[22] Asano K, Iwata T, Irikura K (2005): Estimation of source rupture process and strong ground motion simulation of the 2002 Denali, Alaska, earthquake, *Bull. Seismol. Soc. Am.* ***95***, 5, 1701–1715.

[23] Matsuda T (1975): Magnitude and recurrence interval of earthquakes from a fault, *ZISIN2*, ***28***, 269-283 (in Japanese with English abstract).

[24] Takemura T (1990): Magnitude-seismic moment relations for the shallow earthquakes in and around Japan, ZISIN2, ***43***, 257-265 (in Japanese with English abstract).

[25] Wesnousky SG (2008): Displacement and geometrical characteristics of earthquake surface ruptures: issues and implications for seismic-hazard analysis and the process of earthquake rupture, *Bull. Seismol. Soc. Am.*, ***98***, 4, 1609-1632.

[26] Ishimura D, Okada S, Niwa Y, Toda S (2015): The surface rupture of the 22 November 2014 Nagano-ken-hokubu earthquake (Mw 6.2), along the Kamishiro fault, Japan, *Active Fault Research*, ***43***, 95-108.

[27] Shirahama Y., Yoshimi M, Awata Y, Maruyama T, Azuma T, Miyashita Y, Mori H, Imanishi K, Takeda N, Ochi T, Otsubo M, Asahina D, Miyakawa A (2016): Characteristics of the surface ruptures associated with the 2016 Kumamoto earthquake sequence, central Kyushu, Japan, *Earth, Planets and Space*, ***68***, 191, https://doi.org/10.1186/s40623-016-0559-1.

[28] Japan Seismic Hazard Information Station (J-SHIS) (2019): Deep subsurface structural physical properties API. http://www.j-shis.bosai.go.jp/en/api-dstruct-phys#request-parameter.

[29] Abrahamson NA (2002): Velocity pulses in near-fault ground motions, *in Proceeding of the UC Berkeley-CUREE symposium in Honor of Ray Clough and Joseph Penzien*: *Consortium of Universities for Research in Earthquake Engineering*, 40-41, Berkeley, California.

[30] Bray JD, Rodriguez-Marek A (2004): Characterization of forward-directivity ground motions in the near-fault region, *Soil Dynamics and Earthquake Engineering*, ***24***, 815-828.

[31] Burks LS, Baker JW (2016): A predictive model for fling-step in near-fault ground motions based on recordings and simulations, *Soil Dynamics and Earthquake Engineering*, ***80***, 119-126.

[32] Nakamura H, Miyatake T (2000): An approximate expression of slip velocity time function for simulation of near-field strong ground motion, *ZISIN2*, ***53***, 1–9 (in Japanese with English abstract).

[33] Day SM (1982): Three-dimensional simulation of spontaneous rupture: The effect of nonuniform prestress, *Bull. Seismol. Soc. Am*, ***72***, 1881–1902.

[34] Headquarters for Earthquake Research Promotion (HERP) (2017): Report: 'National Seismic Hazard Maps for Japan (2017)', https://www.jishin.go.jp/main/chousa/17_yosokuchizu/yosokuchizu2017_chizu_3.pdf (in Japanese).

[35] Headquarters for Earthquake Research Promotion (HERP) (2018): Report: 'National Seismic Hazard Maps for Japan (2018)', https://www.jishin.go.jp/main/chousa/18_yosokuchizu/yosokuchizu2018_chizu_3.pdf (in Japanese).

